

# Wide Voltage-Regulation Range Synchronous-Rectifier LLC Converter with Novel Operation Modes

Xiang Zhou, *Senior Member, IEEE*, Jiarui Wu, *Student Member, IEEE*, Huan Luo, *Member, IEEE*,

Zihao Song, Long Pei, *Student Member, IEEE*, Donghua Duan, Peng Guo, *Member, IEEE*,

Laili Wang, *Senior Member, IEEE*, Yan-Fei Liu, *Fellow, IEEE*

**Abstract**—Traditionally, the energy feedback in synchronous rectifier (SR) LLC converter was once considered to only have the ability to reduce the voltage gain. In this paper, a kind of special energy feedback caused by the novel operation modes of LLC resonant converter is proposed for improving voltage gain. Compared to the P, O, and N stages in conventional LLC converter, the stage F is built by controlling the turn-on early time of the synchronous rectifier. By using the proposed operation modes, not only zero-voltage switching (ZVS) of the primary-side and secondary-side switches both are achieved, but the voltage gain of the LLC converter can be increased significantly with a narrow switching frequency range and a smaller magnetizing inductance circulating current. In addition, the proposed operation modes are simple and easy to be utilized in full-bridge, half-bridge, etc., all kinds of LLC converters, thus can form a new general control strategy of the SR LLC. Finally, a 100W half-bridge SR LLC dc-dc converter prototype with a wide voltage-regulation range is implemented to validate the proposed operation modes and the theoretical analysis.

**Keywords**—LLC dc-dc converter, Synchronous rectifier, Wide voltage-regulation range, Narrow switching frequency range.

## I. INTRODUCTION

Recently, along with the rapid development of electric vehicles (EVs), fast EV charger, on-board converter (OBC) and on-board low-voltage dc-dc converter (LDC) are essential in EVs. Generally, EV batteries can be either 400V (with a range of 150 to 500V) or 800V (with a range of 300 to 1000V). As shown in Fig. 1(a), for OBC, an

Manuscript received Aug 20, 2024; revised Oct 22, 2024, and Dec 22, 2024; accepted Feb 21, 2025. This work was supported by the National Natural Science Foundation of China under Grant 52407218, in part by the Open Fund of the State Key Laboratory of High-Efficiency and High-Quality Conversion for Electric Power (No. 2024KF009). (*Corresponding Author: Laili Wang*)

X. Zhou, J. Wu, Z. Song, L. Pei, D. Duan, L. Wang are with the State Key Laboratory of Electrical Insulation and Power Equipment, Xi'an Jiaotong University, Xi'an 710049, China; State Key Laboratory of High-Efficiency and High-Quality Conversion for Electric Power. (e-mail: zhouxiang06@xjtu.edu.cn; wujiarui123@stu.xjtu.edu.cn; zihao.song@stu.xjtu.edu.cn; pl0823@stu.xjtu.edu.cn; 564752335@qq.com; llwang@mail.xjtu.edu.cn).

H. Luo is with College of Electrical Engineering, Sichuan University, Chengdu 610064, China (e-mail: luohuan2387@163.com).

P. Guo is with State Key Laboratory of High-Efficiency and High-Quality Conversion for Electric Power, Hunan University, Changsha 410082, China (e-mail: pengguo92@hnu.edu.cn)

Y.-F. Liu is with the Department of Electrical and Computer Engineering, Queen's University, Kingston, ON K7L 3N6, Canada (e-mail: yanfei.liu@queensu.ca).

isolated DC-DC converter with a wide output voltage range of 150 to 500V or 300 to 1000V is required. For LDC, an isolated DC-DC converter with a wide input voltage range of 150 to 500V or 300 to 1000V is required. As shown in Fig. 1(b), in order to accommodate both 400 V and 800 V batteries, the DC/DC converter in universal fast EV chargers must cover an extremely wide output voltage range, such as 150 to 1000 V [1]. Therefore, a high-efficiency high-power-density isolated DC-DC converter with wide voltage regulation capability is more and more important in EVs application [2]-[5].

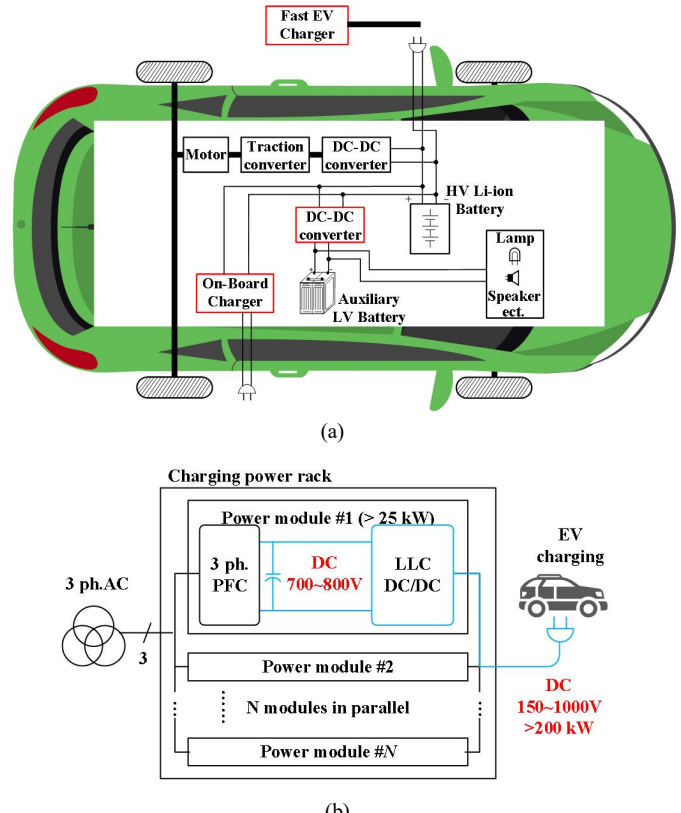


Fig. 1. Diagram of (a) EV charging power rack [1], (b) EV power train [14]

LLC series-parallel resonant converter was first apparent in 1988 in literature [6]-[7], and attracts more and more attention since the 2000s for industrial applications and research [8]-[9]. As one of the most popular isolated dc-dc converters, LLC resonant converter can satisfy the increasing requirement for high-efficiency and high-power-

density switching mode power supply due to the simplest topology and the soft switching of the primary-side switches and secondary-side rectifiers [9]. Although LLC converter has many advantages, it is obviously impossible to cover the various requirement in the different applications. For the wide input and / or output voltage range applications, it is challenging for the LLC converter to achieve wide voltage regulation capability.

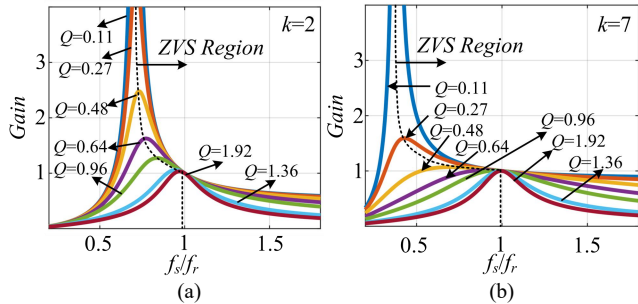


Fig. 2. The voltage gain against switching frequency with different  $k$  and  $Q$   
(a)  $k=2$  and (b)  $k=7$

Fig. 2 shows the voltage gain against switching frequency with different resonant inductance ratio  $k$  and quality factor  $Q$  based on the fundamental harmonic approximation, where  $k$  and  $Q$  are defined in [9], as bellow:

$$\left\{ k = \frac{L_p}{L_r}, Q = \sqrt{\frac{C_r}{R_{ac}}}, R_{ac} = \frac{8n^2}{\pi^2} R_o \right. \quad (1)$$

where  $L_r$  is the series resonant inductance,  $C_r$  is the series resonant capacitance,  $L_p$  is the parallel resonant inductance,  $n$  is the turns ratio of the transformer, and  $R_o$  is the load resistance.  $k$  is generally used to describe the capability of the step-up voltage gain, and the  $Q$  is generally used to describe the relationship between the load and the resonant parameters in LLC converter. From Fig. 2, the characteristic of the parallel resonance is more and more obvious in LLC converter when  $k$  is decreased, thereby obtaining a high step-up voltage gain; the characteristic of the series resonance is more and more obvious in LLC converter when  $k$  is increased, thereby lost the capability of the step-up voltage gain. As the pulse frequency modulation (PFM) is used to regulate the output voltage in traditional LLC converter, thereby causing the drawback as follows.

Firstly, the wide normalized step-up and step-down voltage-regulation ranges are realized by the extremely wide switching frequency variation range, which brings difficulties to the design of magnetic components and driver circuits [10].

Secondly, from Fig. 2, along with a increased  $Q$  value, the voltage gain decreases significantly, which means that the voltage gain decreases sharply along with an increased load. To get the peak voltage gain and improve the step-up capability, the switching frequency should be reduced to lower than  $f_r$ , where  $f_r$  is the resonant frequency between the series resonant capacitance  $C_r$  and the the series resonant inductance  $L_r$ . However, if the switching frequency reaches the operating point to achieve peak voltage gain, the gain-frequency curves are prong to non-monotonous around this point, and LLC converter may be operating at a hard-

switching region, thereby bringing control instability issue and lost soft switching characteristic [11]. Therefore, the step-up voltage gain of LLC converter is limited at full load condition.

Thirdly, according to Fig. 2, a small  $k$  value could help to improve voltage gain and shrink the switching frequency range with the same circuit parameters and load conditions. Although a small parallel resonant inductance  $L_p$  is good for wide voltage range applications, a high circulating current and high turn-off current would cause high conduction and switching loss, thereby degrading the system efficiency of the LLC converter [12].

Along with the wide voltage-regulation range applications develop rapidly, such as electric vehicle (EV) chargers, power delivery (PD) adapters, photovoltaic dc-dc converters, fuel cell power systems, etc., a single conventional LLC converter cannot satisfy the requirements of these applications directly as the voltage gain curve at the inductive region is very flat under heavy load and the capability of the step-up voltage gain of LLC converter is also weak [10]-[12]. Therefore, it is urgent and necessary to expand the voltage-regulation capacity and enhance the competitiveness of the LLC converter in wide input and / or output voltage range applications.

In [13]-[14], the operation modes of the conventional LLC resonant converter are analyzed and the peak gain point is present. By designing the circuit parameters with a small resonant inductance ratio  $k$ , the capacity of the step-up voltage gain can be improved slightly [15]-[16]. However, a small  $k$  means a small magnetizing inductance and a high circulating current, which increases conduction loss and copper loss and degrades the converter efficiency. In [17]-[19], primary-side or secondary-side phase-shift LLC converters are presented, and the wide voltage gain can be achieved by adjusting the phase-shift angle. In these converters, the soft-switching condition is relative to the load current and phase-shift angle, thus, it is difficult to achieve soft-switching under the high step-up or step-down output voltage with light load.

To achieve a higher voltage gain, some extra switches are added to LLC converter to form a Boost cell that operates with pulse width modulation (PWM) control [20]-[21]. However, adding components will inevitably increase extra cost and complexity, and soft switching will be lost under PWM control strategy. Recently, the primary full bridge (FB) / half bridge (HB) hybrid operation modes LLC converter is presented to enhance the step-up voltage gain capacity [22]-[24]. Due to the voltage gain of FB LLC converter being two times that of HB LLC converter under resonant frequency point, by using the topology-reconfigurable primary side to make the LLC converter operates at different modes, the voltage-regulation range can be broadened significantly [24]. Similarly, a topology-reconfigurable secondary rectifier can also make the LLC converter operates at different modes to improve the voltage-regulation range [25]-[26]. In these FB and HB hybrid control LLC converters, the FB circuit and some extra switches are required in the primary or secondary side, which increases the cost and control complexity. In addition, when the operation mode is changed between FB and HB,

the switching frequency jumps sharply, which causes a large output voltage oscillation and deteriorates the dynamic characteristic. As the switching frequency of each switch is different under the different operation modes, thus the loss and the temperature among these switches are not balanced, which needs to be optimized to improve reliability and extend life [27]. In [28]-[29], the topology-reconfiguration transformers can help to improve output voltage regulation capability in LLC converter. However, the extra transformer or switches would increase the cost and complexity of the converter.

In decades, synchronous rectifier (SR) technology is more and more popular in LLC converters to reduce the conduction loss of the secondary side and improve efficiency. As a consequence, a new degree of freedom can be adopted on SR switches. In [30], by adjusting the phase shift angle of the SR switches in LLC converter, the resonant inductor can be used as the Boost inductor, and the output voltage gain is improved along with an increased equivalent duty cycle in Boost cell. However, the ZVS turn-on of the SR switches is lost by using this scheme, which increases the secondary side switching loss. In [31]-[33], the control scheme that makes turn-off time delay of SR switches is proposed, which results that the energy is transformed to the primary side, and the ZCS turn-off of the SR switches is lost by using this scheme.

In this paper, the novel operation modes of LLC converter are proposed by controlling the turn-on early time of SR to achieve the energy feedback and high voltage gain with ZVS turn-on and ZCS turn-off of SR switches, which are suitable for the wide voltage-regulation range applications. The novelty and the advantages of the proposed LLC converter lie in 1) the novel operation modes consisting of stage F are proposed and elaborated; 2) without any adding components, the voltage gain is increased significantly along with an increasing leading angle of SR switches. Therefore, by the proposed novel operation modes, the switching frequency range is squeezed significantly, which is good for the design of the magnetic components. Compared to the conventional LLC converter, the large magnetizing inductance could be designed to reduce the circulating current if the same voltage gain is required. 3) soft switching can be achieved in the primary sides easily due to the higher current through the resonant inductor when the primary switches are turned off; 4) soft switching can be achieved in the secondary sides due to voltage ringing across the SRs; 5) the peak voltage of the resonant capacitor, and the peak currents of the transformer primary and secondary winding are reduced when the switching frequency is smaller and far away from the resonant frequency, which can reduce the stress of the devices; 6) the advantages of conventional LLC converter are kept, such as simple circuit structure and control strategy, the same switching frequency among the switches and the balanced loss, and the proposed operation modes are easy to be used in all kinds of SR LLC converter.

## II. NOVEL RESONANT STAGE OF SR LLC CONVERTER

In the conventional SR LLC converter, the operation modes consisting of P, O, and N stages have been studied

and made a detailed analysis [11]-[12]. From [11], OPO, PO, PON, NP, PN, and NOP are the six major operation modes in LLC converter, generally. To achieve high efficiency and soft switching, PO mode is the popular design for the LLC converter [11]. The half-bridge SR LLC converter is shown in Fig. 3, and the turns ratio of the transformer is  $N_1: N_2: N_3 = n: 1: 1$ , where  $N_1$  is the turns of the primary winding,  $N_2$  and  $N_3$  are the turns of the secondary windings. The key waveforms of the conventional SR LLC converter with PO mode are shown in Fig. 4, where  $i_{Lr}$  is the current flowing through the series resonant inductance,  $i_{Lm}$  is the current flowing through the parallel resonant inductance (the magnetizing inductance of the transformer  $L_m$  is generally used as the parallel resonant inductance  $L_p$  in LLC converter).

According to [11], when  $Q_1$  is turned on and  $Q_2$  is turned off, there are P, O, and N three resonant stages depending on the voltage across the magnetizing inductor, as shown in Fig. 5(a)-(c). In a traditional LLC converter, the energy is always transferred from input to output in P stage or N stage, or no energy is transferred to output in O stage, thus the resonant stages only depend on the voltage across the magnetizing inductor.

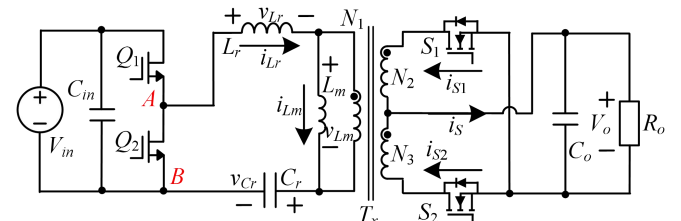


Fig. 3. The HB SR LLC converter

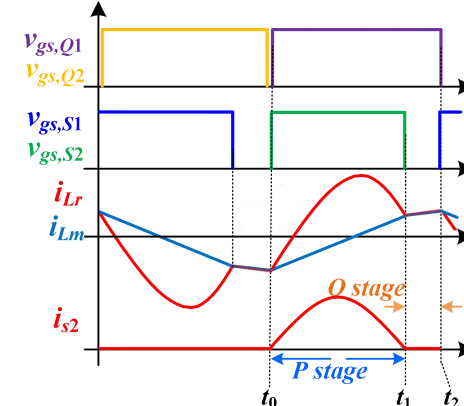


Fig. 4. The operation waveforms of the conventional LLC converter

However, when the active switches in SR are used as the master switches, the operation modes of the LLC converter could be changed. The energy can be stored in the primary inductor or feedbacked from output to input, and the resonant stages depend on the voltage across the magnetizing inductor and the current flow through the load. Thus, the different operation stages in LLC converter are shown in Fig. 5.

According to [30], when the LLC converter operates at P or N stage, the transformer secondary can be shorted by the SR switches, thereby the resonant inductor is charged and the energy is stored in the resonant inductor. Therefore, the conventional P or N stage can be converted to the operation

stage in [30] by using SR switches, which is shown in Fig. 5(d).

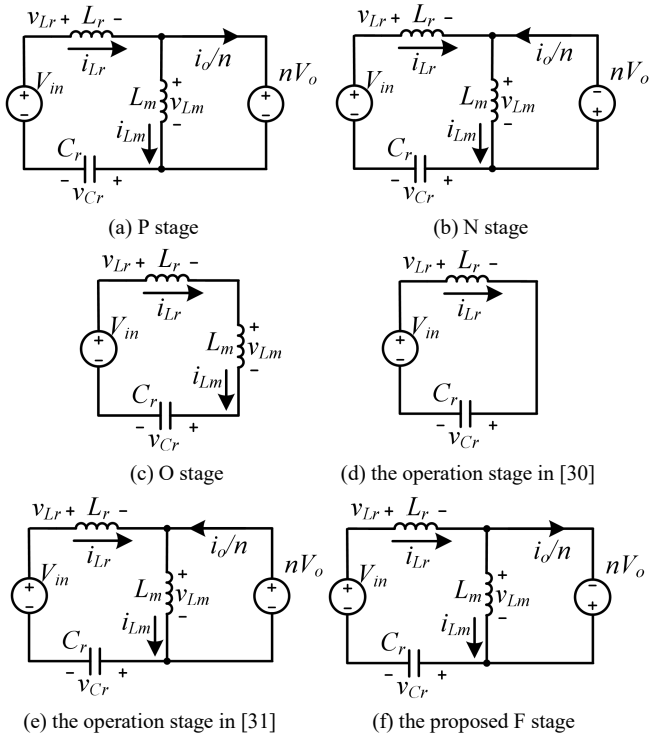


Fig. 5. The equivalent circuits of the different operation stages in LLC converter

When the LLC converter operates from P stage to O stage, the SR switches should have been turned off. However, if the SR switches are turned off delay, the conventional O stage is converted to the operation stage in [31]. The equivalent circuit is shown in Fig. 5(e), and the key waveforms are shown in Fig. 6. As SR switches are turned off at time  $t_1$  instead of  $t_0$  when the switching frequency of the LLC converter is lower than the resonant frequency, the energy is feedbacked from output to input, thus the voltage gain is reduced. Although ZCS turn-off of the SR switches is lost by using these schemes, the high step-down voltage regulation capability is obtained. Consequently, the energy feedback in SR-LLC converter was once considered traditionally only to have the ability to reduce the voltage gain.

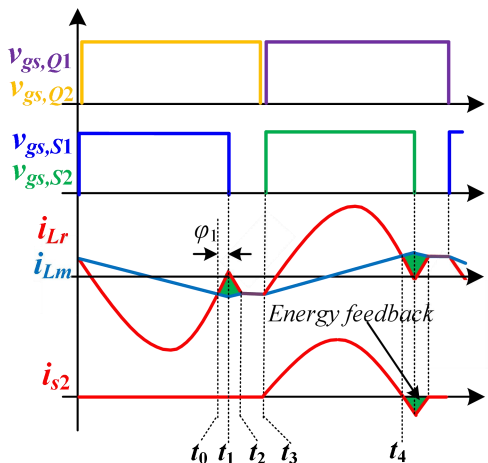


Fig. 6. The operation waveforms of the LLC converter in [31]

In [34], the voltage ringing across SR switches is elaborated. However, the effect of turn-on early of SR switches is not analyzed, and the circuit parameters design method is just given to avoid the turn-on early of SR switches in [34]. Thus, it is considered traditionally that only can reduce the voltage gain and cause a large circulating current to deteriorate the efficiency. Based on the effort in [34], the effect of turn-on early of SR switches is elaborated in this paper. The research effort shows that the voltage gain can be improved, the soft-switching characteristics of all the switches can be kept by turn-on early of SR switches, and the efficiency is not always reduced, which is totally different from the conventional wisdom.

Fig. 7 shows the key waveforms of the proposed HB SR LLC converter with F stage. During  $t_0 \sim t_2$ , the SR switch  $S_2$  is turned on at  $t_2$  in the conventional LLC converter, and the period  $t_0 \sim t_2$  is defined as O stage. If the SR switch  $S_2$  is turned on early at  $t_1$ , O stage is reduced from  $t_0 \sim t_2$  to  $t_0 \sim t_1$ . The energy is feedbacked from output to input, and the load current flows out of load during  $t_1 \sim t_2$ . Thus, the operation during  $t_1 \sim t_2$  is defined as F stage in this paper, and the conventional O stage during  $t_1 \sim t_2$  is converted to F stage. Here  $\alpha = 360^\circ \times (t_2 - t_1)/T_s$  represents SR switches leading angle. The equivalent circuit of F stage is shown in Fig. 5(f). As a sequence, the current  $i_{Lr}$  is increased by F stage, and ZVS turn-on of switches  $Q_1$  and  $Q_2$  can be achieved easily at  $t_6$  and  $t_2$  due to a higher current  $i_{Lr}$ .

As aforementioned analysis, O stage can be converted to F stage by turn-on early of SR switches. However, along with the load current increased, if N stage occurs, F stage would be lost and is the same as N stage. Therefore, F stage is degenerated to N stage, because SR switches should have been conducted early at N stage.

In the traditional SR LLC converter, the voltage across SR switches is not zero during  $t_0 \sim t_2$ , thus the turn-on early of SR switches will lose zero-voltage-switching (ZVS), causing high switching loss. In [34], by designing the circuit parameters properly, the voltage ringing across SR switches could help to achieve ZVS during  $t_0 \sim t_2$ . As shown in Fig. 7, when the voltage ringing reaches zero at  $t_1$ , turn-on early switch  $S_2$  can achieve ZVS. According to [34], the voltage across SR switches  $v_{ds,S2}$  during  $t_0 \sim t_2$  can be expressed as

$$v_{ds,S2}(t-t_0) = \frac{V_o}{2} - \frac{K}{2n(K+1)} \left[ \left( -2nV_o + V_{in} + \frac{V_o^2}{4C_r R_o V_{in} f_s} \right) \cos \omega_p(t-t_0) + \frac{nV_o \pi \sqrt{K+1}}{2K} \sin \omega_p(t-t_0) \right] + \left[ \frac{V_o}{2} + \frac{K}{2n(K+1)} \left( -2nV_o + V_{in} + \frac{V_o^2}{4C_r R_o V_{in} f_s} \right) \right] \cos \omega_h(t-t_0). \quad (2)$$

where  $K$ ,  $\omega_r$ ,  $\omega_p$  and  $\omega_h$  satisfy

$$\left\{ \begin{array}{l} \omega_h = \frac{1}{\sqrt{(L_r + L_m) \times C_{oss} + C_p}} \\ \omega_p = \frac{1}{\sqrt{(L_r + L_m)C_r}}, K = \frac{L_m}{L_r}, \omega_r = \frac{1}{\sqrt{L_r C_r}} \end{array} \right.$$

where  $C_p$  is the parasitic paralleled capacitance of the transformer and  $C_{oss}$  is the parasitic output capacitance of the SR switches. Hence, ZVS of SR switches can be guaranteed by a simple circuit parameters design.

FIG. 8 shows the qualitative diagram of the apparent input power of LLC converter with SR switches turn-off delay or turn-on early.  $A_Q$  represents that the area enclosed by the current  $i_{Lr}$  and time axis. Where  $T_s$  is the switching period,  $P_o$  is active output power, and  $Q_{Lm}$  is reactive power caused by the magnetizing inductor. The following assumption are made: 1) the active power  $P_{in}=P_o$ ; 2)  $Q_{Lm}$  is the same in the three operation mode as shown in Fig. 8; 3) the current  $i_{Lm}$  is the same at the end of P stage in the three operation mode as shown in Fig. 8.

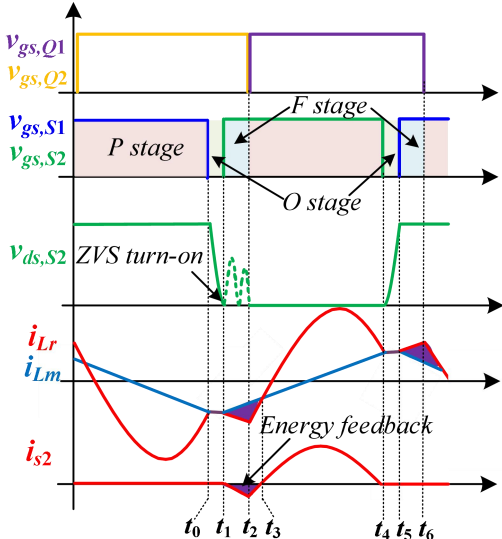


Fig. 7. The key waveforms of the HB SR LLC converter with F stage

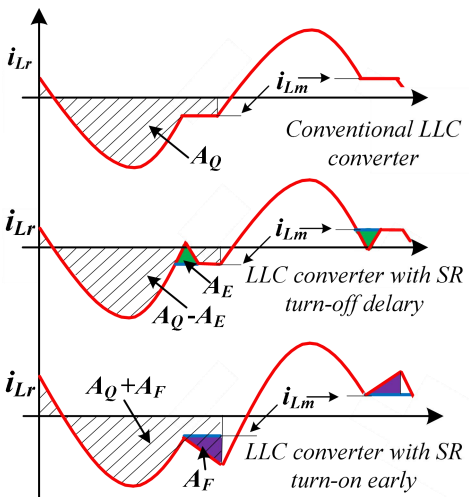


Fig. 8. The qualitative diagrams of the apparent input power of LLC converter with SR switches turn-off delay or turn-on early

Therefore, in the conventional LLC converter, when switch  $Q_2$  is conducted, the apparent input power of LLC converter  $S_{in}$  can be expressed as in (3). From Fig. 8, compared to the conventional LLC converter, the apparent input power  $S_{in}$  is reduced by the SR switches turn-off delay, because the area enclosed by the current  $i_{Lr}$  and time axis is reduced by  $A_E$ . Compared to the conventional LLC converter, the apparent input power  $S_{in}$  is increased by the SR switches turn-on early, because the area enclosed by the current  $i_{Lr}$  and time axis is increased by  $A_F$ .

$$S_{in} = \frac{V_{in} \times 2 \int_0^{T_s} i_{Lr} dt}{T_s} = \frac{2V_{in} A_Q}{T_s} = \sqrt{P_o^2 + Q_{Lm}^2} = \sqrt{\left(\frac{V_o}{R_o}\right)^2 + Q_{Lm}^2} \quad (3)$$

As a qualitative result, according to (3), the output voltage is increased when the SR switches is turned on early, and the output voltage is decreased when the SR switches is turned off delay.

As only O stage can be modified as F stage and PO mode is the most favorable operation mode of the LLC [11], the PO mode is selected as an example to analyze in this paper.

### III. THE OPERATION MODES AND CHARACTERISTIC ANALYSIS

#### A. The operation modes and voltage gain analysis

Fig. 9 shows the waveforms of POF mode within the positive half switching-cycle ( $t_2 \sim t_6$  in Fig. 7).

During the state P, the current flowing through resonant inductor  $L_r$  and magnetizing inductor  $L_m$ , as well as the voltage across the resonant capacitor  $C_r$  can be described as :

$$\left\{ \begin{array}{l} i_{LrP}(t) = I_{LrP} \sin(\omega_r t - \varphi_p) \\ i_{LmP}(t) = -I_m + \frac{NV_o}{L_m} t \\ v_{CrP}(t) = v_{ab} - NV_o - L_r \frac{di_{LrP}}{dt} \end{array} \right. \quad (4)$$

where  $I_{LrP}$  and  $\varphi_p$  are the magnitude and initial phase angle of  $i_{LrP}$  respectively,  $-I_m$  is the initial current of  $i_{LmP}$ ,  $\omega_r = 1/\sqrt{L_r C_r}$  is the angular frequency of series resonance of  $L_r$  and  $C_r$ ,  $N$  is the turn ratio of the transformer,  $v_{ab}$  is the voltage of the resonant tank, which is equal to  $V_{in}$ .

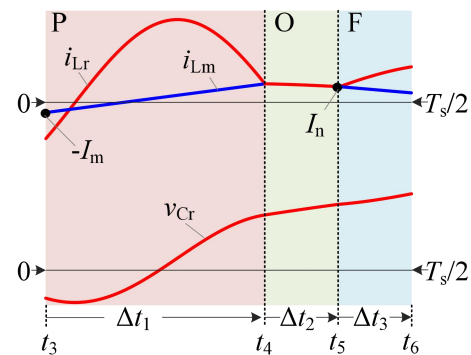


Fig. 9. The waveforms of POF mode

During the state O,  $L_m$  joins the resonance of  $L_r$  and  $C_r$ , and the resonant variables can be obtained as

$$\begin{cases} i_{L_{rO}}(t) = I_{L_{rO}} \sin(\omega_m t - \varphi_0) \\ i_{L_{mO}}(t) = i_{L_{rO}}(t) \\ v_{CrO}(t) = v_{ab} - (L_r + L_m) \frac{di_{L_{rO}}}{dt} \end{cases} \quad (5)$$

where  $I_{L_{rO}}$  and  $\varphi_0$  are the magnitude and initial phase angle of  $i_{L_{rO}}$  respectively, and  $\omega_m = 1/\sqrt{(L_r+L_m)C_r}$  is the angular frequency of series resonance of  $L_r$ ,  $L_m$  and  $C_r$ .

During the state F, the corresponding resonant variables can be obtained as

$$\begin{cases} i_{L_{rF}}(t) = I_{L_{rF}} \sin(\omega_i t - \varphi_F) \\ i_{L_{mF}}(t) = I_n - \frac{NV_o}{L_m} t \\ v_{CrF}(t) = v_{ab} + NV_o - L_r \frac{di_{L_{rF}}}{dt} \end{cases} \quad (6)$$

where  $I_{L_{rF}}$  and  $\varphi_F$  are the magnitude and initial phase angle of  $i_{L_{rF}}$  respectively,  $I_n$  is the initial current of  $i_{L_{mF}}$ .

When the converter moves from one state to its adjacency state, the current through the resonant inductor and the voltage across the resonant capacitor cannot change suddenly. Therefore, the continuity condition for the resonant current can be expressed as

$$\begin{cases} i_{L_{rP}}(\Delta t_1) = i_{L_{rO}}(0) \\ i_{L_{mP}}(\Delta t_1) = i_{L_{rO}}(0) \\ i_{L_{rO}}(\Delta t_2) = i_{L_{rF}}(0) \\ i_{L_{rO}}(\Delta t_2) = i_{L_{mF}}(0) \end{cases} \quad (7)$$

where  $\Delta t_1$ ,  $\Delta t_2$  and  $\Delta t_3$  are the durations of state P, state O and state F, respectively, which meet

$$\Delta t_1 + \Delta t_2 + \Delta t_3 = T_s / 2 \quad (8)$$

Similarly, the continuity condition for the resonant capacitor voltage can be expressed as

$$\begin{cases} v_{CrP}(\Delta t_1) = v_{CrO}(0) \\ v_{CrO}(\Delta t_2) = v_{CrF}(0) \end{cases} \quad (9)$$

By the symmetry of the half-bridge LLC converter, the end value of the current should be opposite to the initial value within a half switching cycle. Therefore, the symmetry condition for the resonant current and the magnetizing current can be described as

$$\begin{cases} i_{L_{rP}}(0) + i_{L_{rF}}(\Delta t_3) = 0 \\ i_{L_{mP}}(0) + i_{L_{mF}}(\Delta t_3) = 0 \end{cases} \quad (10)$$

For the symmetry condition for resonant capacitor voltage, the sum between the end value and the initial value of  $v_{Cr}$  should be equal to  $v_{ab}$  within a half switching cycle.

$$v_{CrP}(0) + v_{CrF}(\Delta t_3) = v_{ab} \quad (11)$$

The average current following through switch  $Q_1$  over one switching cycle is equal to the input current, thus the input power can be obtained as

$$P_{in} = V_{in} \cdot I_{in} = \frac{V_{in}}{T_s} \left( \int_0^{\Delta t_1} i_{L_{rP}} dt + \int_0^{\Delta t_2} i_{L_{rO}} dt + \int_0^{\Delta t_3} i_{L_{rF}} dt \right) \quad (12)$$

The output power can be similarly obtained as

$$P_o = \frac{2NV_o}{T_s} \left[ \int_0^{\Delta t_1} (i_{L_{rP}} - i_{L_{mP}}) dt + \int_0^{\Delta t_3} (i_{L_{mF}} - i_{L_{rF}}) dt \right] \quad (13)$$

The assumption of  $P_{in}=P_o$  is made. Then, by substituting (3~5) into (6~12), and taking  $V_o$ ,  $V_{in}$ ,  $P_o$  and  $\Delta t_3$  as known parameters, 12 transcendental equations can be obtained to solve for the corresponding switching frequency  $f_s$ , as well as other current and voltage variables, including  $I_{L_{rP}}$ ,  $I_{L_{rO}}$ ,  $I_{L_{rF}}$ ,  $I_m$ ,  $I_n$ ,  $\varphi_P$ ,  $\varphi_O$ ,  $\varphi_F$ ,  $\Delta t_1$ ,  $\Delta t_2$ . Therefore, the voltage gain of the SR LLC converter with POF mode can be shown in Fig. 10. When the SR switches leading angle  $\alpha$  is zero, the LLC converter operates at conventional PO mode. Along with the leading angle  $\alpha$  increasing, O stage is reduced and modified as F stage, and the voltage gain is increased gradually at the same switching frequency. Finally, the whole O stage is modified as F stage, and the converter operates at PF mode.

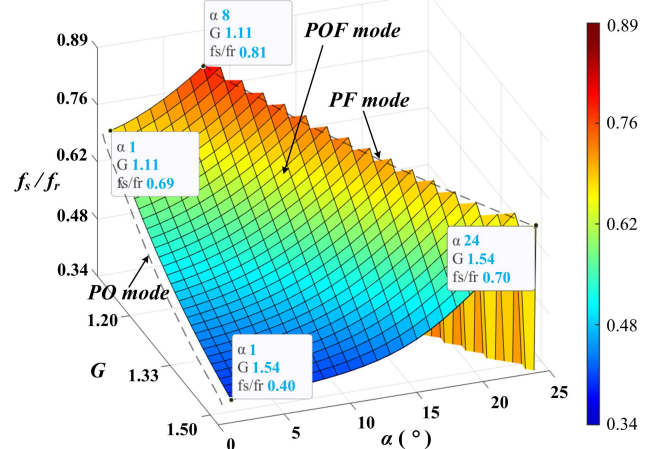


Fig. 10. The relationship among the voltage gain, switching frequency, and the SR switches leading angle

## B. The circuit characteristic analysis

When the resonant components are  $L_r=10\mu H$ ,  $L_m=120\mu H$ ,  $C_r=120nF$ , the turns ratio of the transformer is 5:1:1, the output voltage is 12V, and the load current is 8A, the relationship among the voltage gain, switching frequency and the SR switches leading angle is shown in Fig. 10. And the comparisons of the voltage gain and current between PO and PF modes are shown in Fig. 11 and Fig. 12. The peak voltage and current comparisons are shown in Fig. 13.

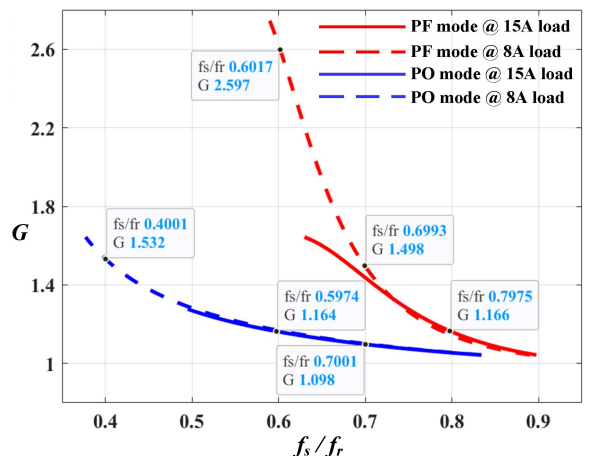


Fig. 11. The comparison of the voltage gain between PO and PF modes

As shown in Fig. 11, when the load current is 8A, the voltage gain of the LLC converter operating at PF mode is 2.23 times of that at PO mode at  $f_s/f_r=0.6$ , and the switching frequency range of the PF mode LLC converter is 50% reduced compared to PO mode LLC converter at around the voltage gain  $G=1.5$ . Moreover, the voltage gain can reach to  $G=2.74$  at PF mode, but only 1.64 is obtained at PO mode even though the switching frequency is much lower.

From Fig. 12, the primary and secondary currents in PO mode are slightly smaller than that in PF mode under 8A load current. However, along with the load current increasing, the switching frequency is required to be far away from the resonant frequency  $f_r$  to keep the same voltage gain in LLC converter. As a consequence, the time interval of P stage is reduced and the O stage is extended. Therefore, the peak value of the primary and secondary current is increased significantly to ensure that the average value of secondary current  $i_S$  is equal to the load current, which causes a high root mean square (RMS) value of the primary and secondary currents in the LLC converter with PO mode, thereby the conduction loss increased. As shown in Fig. 9, although there is feedback current during F mode, the time interval of energy transferred into the secondary

side is still increased as O stage is reduced. Hence, the primary and secondary RMS currents in PF mode are even smaller than that in PO mode under heavy load and low switching frequency, such as 15A load current in Fig. 12.

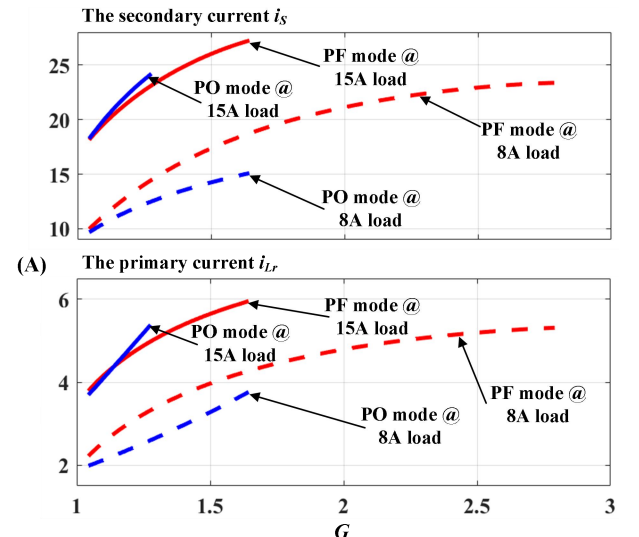


Fig. 12. The comparison of the RMS current between PO and PF modes

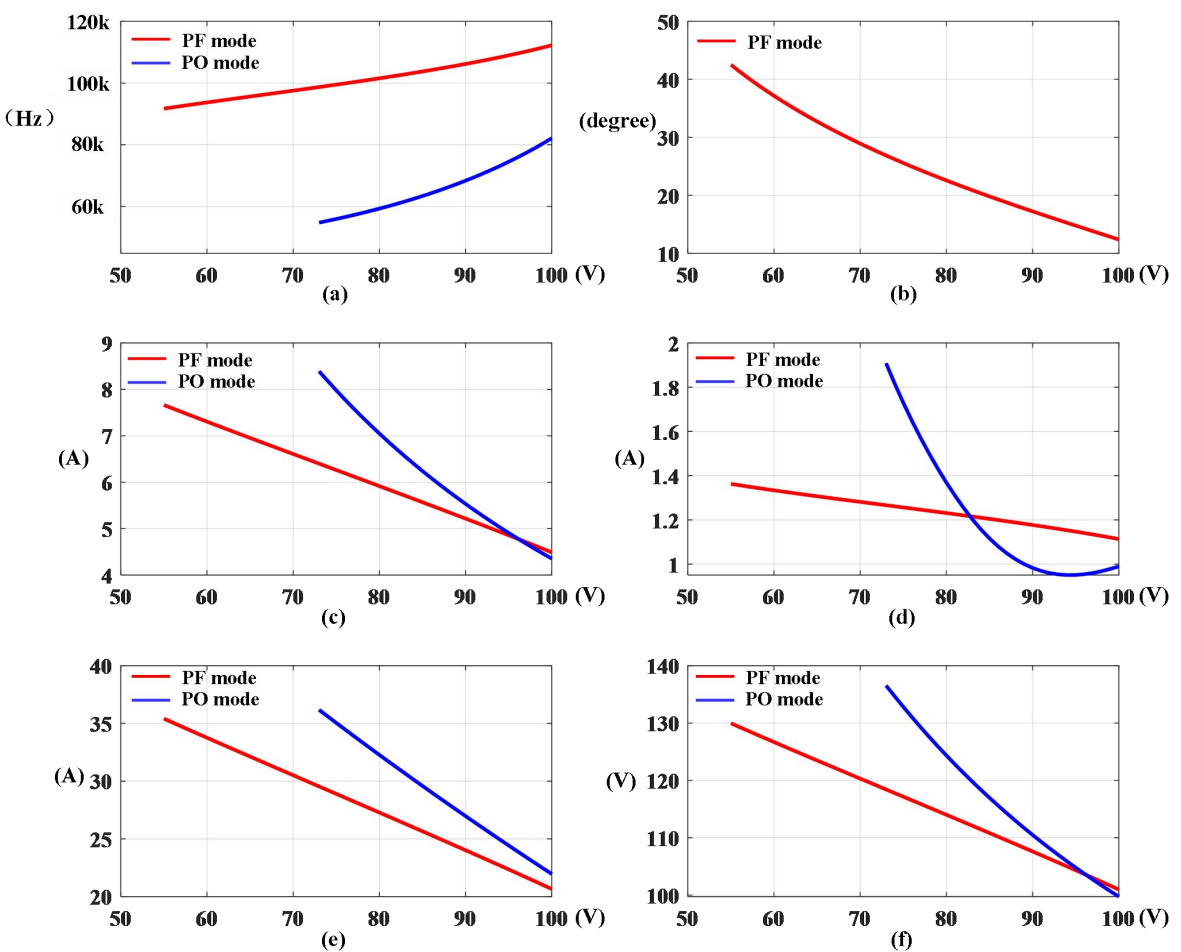


Fig. 13. When  $L=10\mu\text{H}$ ,  $L_m=120\mu\text{H}$ ,  $C=120\text{nF}$ , the turns ratio of the transformer is 5:1:1, 12V/8A output, the comparison of the LLC converter under PO and PF mode when input voltage against (a) switching frequency (b) leading angle  $\alpha$  (c) the peak resonant current  $i_{Lr,max}$  (d) the peak magnetizing current  $i_{Lm,max}$  (e) the peak secondary side current  $i_{S,max}$  (f) the peak resonant voltage  $v_{Cr,max}$

From (4)-(13), the time domain model of the LLC converter is established, thus the comparison of the LLC

converter under PO and PF mode when input voltage against (a) switching frequency (b) leading angle  $\alpha$  (c) the

peak resonant current  $i_{Lr,max}$  (d) the peak magnetizing current  $i_{Lm,max}$  (e) the peak secondary side current  $i_{s,max}$  (f) the peak resonant voltage  $v_{Cr,max}$  are shown in Fig. 13. It can be seen that not only the more narrow switching frequency range and the wider input voltage regulation range are achieved, but the peak values of the current flows through the magnetizing inductor, the current flows through the primary side resonant inductor, the current flows through the secondary side SR switches, and the voltage across primary side resonant capacitor in PF mode are lower than that in conventional PO mode along with the input voltage decreased.

Although the RMS current in PF mode is slightly higher than that in PF mode at 8A load current from Fig. 12, the current stress of the primary and secondary side switches, and the voltage stress of the resonant capacitor can be reduced by the lower peak value of the primary and secondary side current, and resonant voltage  $v_{Cr}$  from Fig. 13.

In LLC converter, the flux density in the high-frequency transformer is a function of magnetizing current and can be expressed as:

$$L_m i_{Lm,max} = N_{Tp} B_{max,Lm} S_T \quad (14)$$

where  $L_m$  is the inductance value of the magnetizing inductor,  $i_{Lm,max}$  is the maximum value of the magnetizing current,  $N_{Tp}$  is the primary winding turns number,  $B_{max,Lm}$  is the peak ac flux density of the magnetizing inductor, and  $S_T$  is the cross-sectional area of the middle leg of the transformer core.

The flux density in the resonant inductor is a function of the primary current and can be expressed as:

$$L_r i_{Lr,max} = N_{Lr} B_{max,Lr} S_{Lr} \quad (15)$$

where  $L_r$  is the inductance value of the resonant inductor,  $i_{Lr,max}$  is the maximum value of the primary current,  $N_{Lr}$  is the turns number of the resonant inductor  $L_r$ ,  $B_{max,Lr}$  is the peak ac flux density of the resonant inductor, and  $S_{Lr}$  is the cross-sectional area of the middle leg of the resonant inductor core.

The common approach that characterizes core losses is the empirical Steinmetz equation, which is expressed as:

$$P_v = k \cdot f_s^\alpha \cdot (B_{max})^\beta \quad (16)$$

where  $k$ ,  $\alpha$ ,  $\beta$  are constants provided by the manufacturer, and  $P_v$  is time-average core loss per unit volume with switching frequency  $f_s$ .

From (14) to (16), the peak ac flux density  $B_{max,Lr}$  is proportional to the current  $i_{Lr}$ , and the peak ac flux density  $B_{max,Lm}$  is proportional to the current  $i_{Lm}$ . From [35], the coefficient  $\alpha$  for ferrite materials N87 is 1.63, the coefficient  $\beta$  for ferrite materials N87 is 2.25. According to Fig. 13, if input voltage is 75V, the core loss of the transformer and the resonant inductor of the proposed converter is around 1.2 to 1.4 times higher than that of the conventional LLC converter as the switching frequency is reduced from 100kHz to 60kHz. Nevertheless, from [40], the output voltage ripple of LLC converter can be calculated as

$$\Delta v_o = R_{ESR,C_o} \times \left( \frac{\pi}{2} - 1 \right) \times I_o + \frac{0.363 I_o}{C_o \times f_s}, \quad (17)$$

where  $I_o$  is the average output current,  $C_o$  is the output capacitance value, and  $f_s$  is the switching frequency. If the switching frequency is decreased from 100kHz to 60kHz, a 1.67 times larger output capacitor is required to keep the same output voltage ripple. Meanwhile, a low switching frequency would also cause a larger size of the EMI filtering stage.

### C. The closed-loop characteristic analysis

As shown in Fig. 10 and Fig. 11, the gain-frequency curve is monotonous by adopting the proposed F mode, thus the closed-loop control can be achieved in the practical applications. To verify the proposed novel operation mode in LLC converter can work with a closed-loop, the logic of the closed-loop control strategy is established, which is shown in Fig. 14.

From Fig. 7, to keep achieving ZVS turn-on of the switches, the leading angle  $\alpha$  is the discrete variable. To simplify the closed-loop control strategy, the SR switches are turned on with ZVS when the first voltage ringing reach to zero in the practical applications by detecting the voltages across SR switches. At this case, O stage is very short and can be neglected, and the LLC converter can be regarded as operating at PF mode.

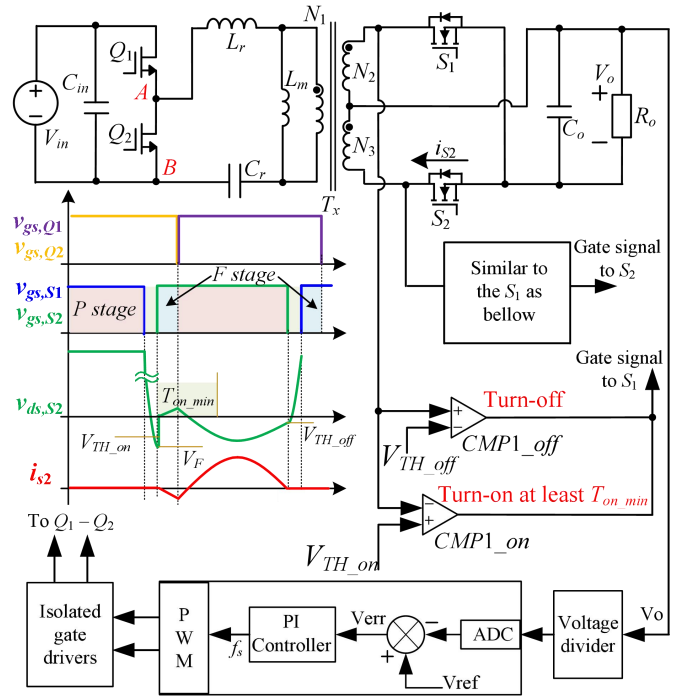


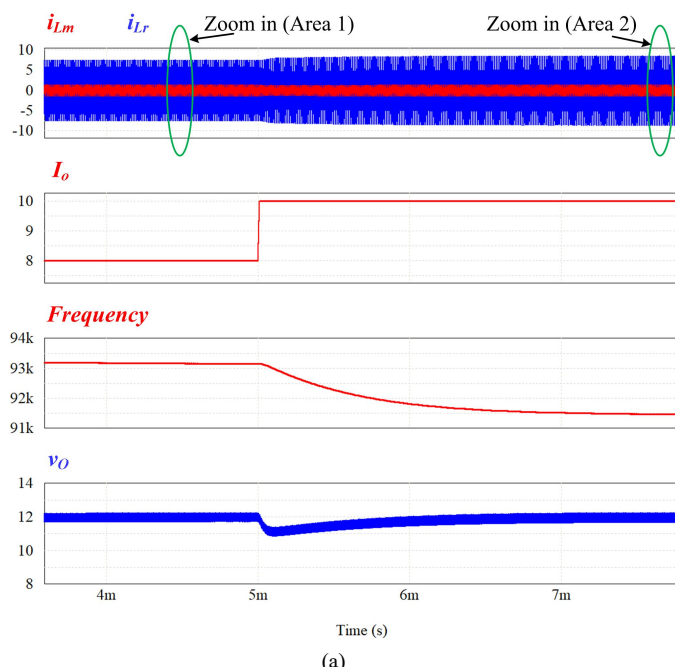
Fig. 14. Closed-loop control strategy of the proposed LLC converter with PF mode

As shown in Fig. 14, when the voltage  $v_{ds,S2}$  decreases to the forward voltage of body diodes  $-V_F$  caused by the voltage ringing at the end of the P stage, the voltage  $v_{ds,S2}$  is lower than the threshold voltage  $V_{TH,on}$ , then the switch  $S_2$  is turned on at least a set value  $T_{on,min}$ . After  $T_{on,min}$ , the secondary-side current flows from source to drain of the switch  $S_2$ , and the voltage across switch  $S_2$  is negative. Along with the

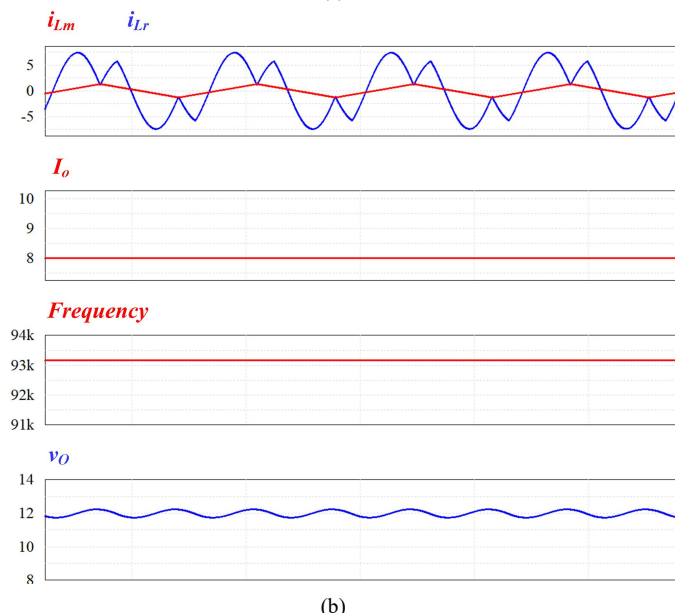
transformer secondary current decreasing to zero, the voltages across SR switches are increased and higher than the threshold voltage  $V_{TH,off}$  eventually, then the switch  $S_2$  is turned off.

According to the control strategy shown in Fig. 14, the simulated closed-loop circuit is built by using PSIM. The dynamic simulated waveforms with the load current step-up from 8A to 10A are given in Fig. 15. As a sequence, the switching frequency is decreased from 93.2kHz to 91.4kHz, the overshoot of the output voltage is less than 1V, and the output voltage is recovered in 1ms.

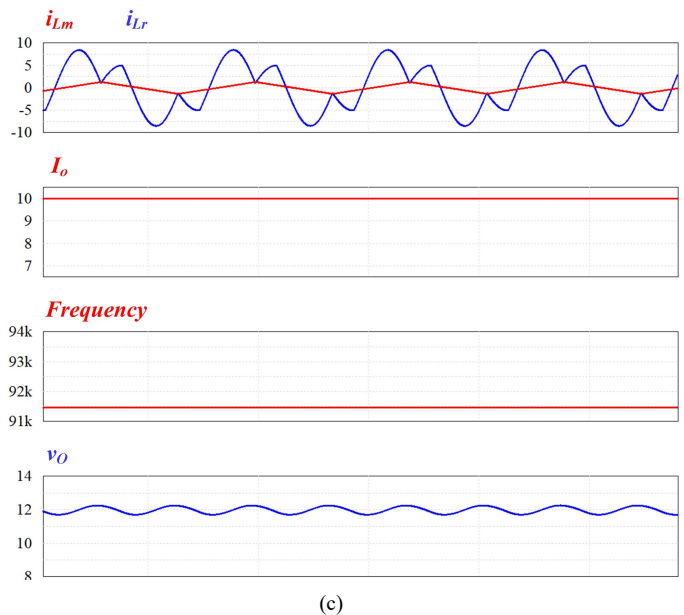
Therefore, the correction and effectiveness of the closed-loop control strategy shown in Fig. 14 can be verified by the simulated results in Fig. 15.



(a)



(b)



(c)

**Fig. 15.** Simulated closed-loop verification when  $L_r=10\mu\text{H}$ ,  $L_m=120\mu\text{H}$ ,  $C_p=120\text{nF}$ ,  $V_{in}=60\text{V}$ , and  $V_o=12\text{V}$  (a) dynamic characteristic of the load current step-up from 8A to 10A (b) steady characteristic with 8A load current (c) steady characteristic with 10A load current

In summary, due to the proposed scheme can improve the voltage-regulation range for the SR half-bridge or full-bridge LLC converter without any topology modification, the converter can be worked at conventional PO mode to keep the high efficiency when a low step-up gain is required or the switching frequency is closing to the resonant frequency. In scenarios with heavy loads and a requirement for high step-up voltage gain, if the voltage-regulation range exceeds the capacity of a traditional LLC converter, the converter can be operated in PF mode using the proposed scheme to cover the wide voltage-regulation range. This negates the necessity of employing two-stage converters or adding auxiliary switches to enhance the voltage-regulation capability. In this paper, the analysis of the novel operation mode of LLC converter is focused on, thus the optimal control strategy including the transition between PF mode and PO mode, small-signal model, digital-control method, etc., would be studied in the future work.

#### IV. EXPERIMENTAL VERIFICATION

From the aforementioned analysis, a SR LLC converter prototype is established to verify the theoretical analysis. The specification and the circuit parameters are shown in Table 1.

Fig. 16 shows the switches  $Q_2$ ,  $S_1$  and current  $i_{Lr}$  experimental waveforms of the SR LLC converter at the same output voltage, and switching frequency. From Fig. 16(a) and (b), the converter operates at PF mode with  $29^\circ$  leading angle, and zero-voltage-switching (ZVS) turn-on can be achieved on the primary side and secondary side, such as the switches  $Q_2$ ,  $S_1$ . From Fig. 16(c) and (d), the converter operates at PF mode with  $19^\circ$  leading angle, and zero-voltage-switching (ZVS) turn-on can be achieved on the primary side and secondary side, such as the switches  $Q_2$ ,  $S_1$ . However, the leading angle is reduced from  $29^\circ$  to  $19^\circ$ .

at F mode, the input voltage increased from 75V in Fig. 16(a) and (b) to 85V in Fig. 16 (c) and (d). As a sequence, the voltage gain can be increased along with the increased leading angle  $\alpha$ , which is consistent with the theoretical analysis.

TABLE I SPECIFICATION AND CIRCUIT PARAMETERS OF THE PROTOTYPE

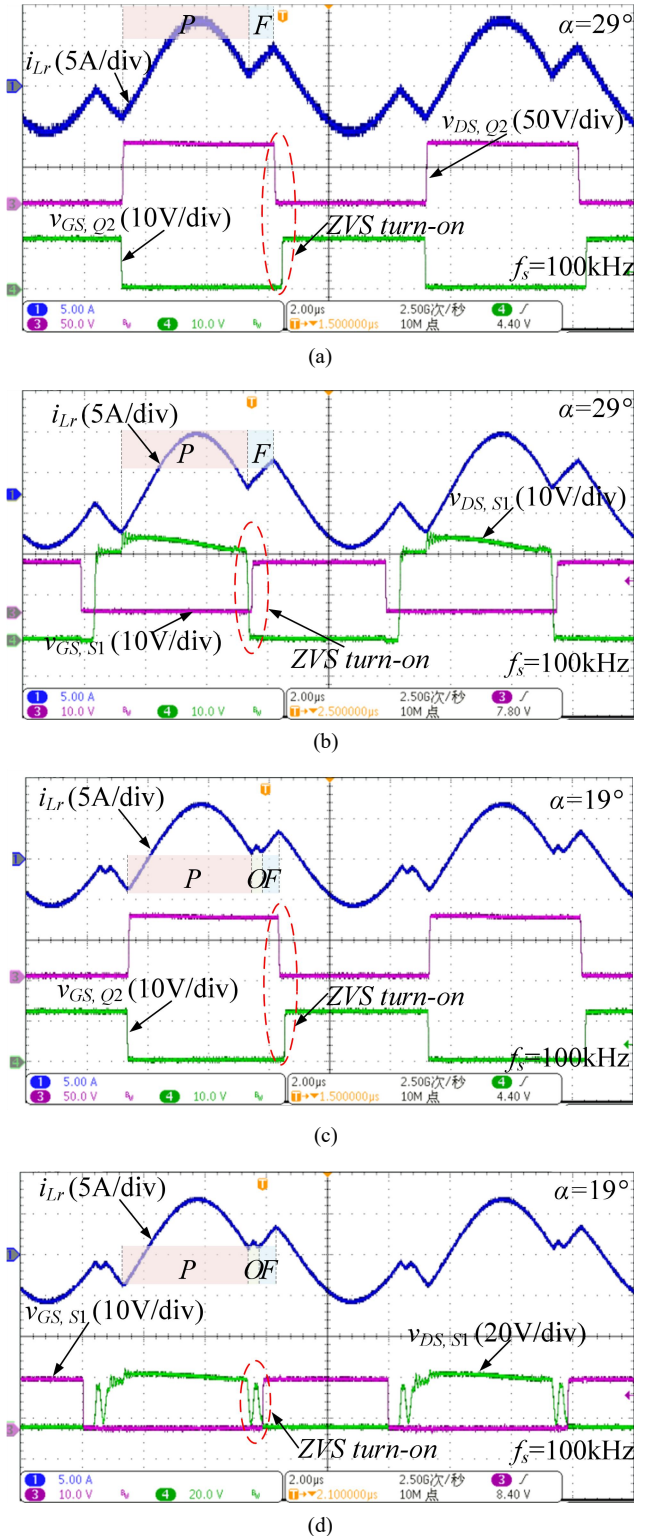
Designators	Part number/Value
Input	54V~115V
Output	12V / 8A
Switching frequency range	87kHz~132kHz
$Q_1 \sim Q_2$	BSC093N15NS5
Primary dead time	200ns
$S_1 \sim S_2$	BSC010N04LS6
Transformer	20: 4: 4, RM12 core, and N87 material, AWG20 Litz wire for the primary winding, AWG18 Litz wire for the secondary winding
$L_m$	118.3μH
$L_r$	9.8μH, RM12 core, and N87 material, AWG18 Litz wire
$C_r$	68nF+47nF+10nF (5% tolerance)
$C_{in}$	10μF×3+56μF
$C_o$	10μF×6+56μF
Controller	TMS320F280048
Driver	SI8233AD-D-IS

From Fig. 16, to achieve ZVS turn-on of the secondary-side switches, the leading angle  $\alpha$  is discontinuous as the SR switches should be turned on at the voltage ringing reaches zero. To simplify the complexity of the control strategy, the SR switches are turned on at the first zero voltage ringing even though the leading angle  $\alpha$  could be used as a free variable, which means the proposed LLC converter operates at PF mode and adopts PFM modulation strategy in this paper. Due to the turn-on time sensing of secondary-side switches in the proposed LLC converter is similar to the controller in [36]-[39], therefore, the new operation mode is focused on, and theoretical analysis is presented in this work.

According to the analysis in [34], the voltage ringing depends on the variables  $L_p$ ,  $C_r$ ,  $C_e$ ,  $R_o$ , and  $f_s$  from (2). The voltage ringing across SR switches will reach zero during the O stage along with an increasing load current (decreasing load resistor  $R_o$ ) [34], thereby ZVS turn-on of SR switches can be achieved under heavy load conditions. However, the voltage ringing is almost higher than zero under light load conditions with a conventional LLC circuit parameter design. Thereby, it is difficult to achieve full ZVS turn-on of SR switches under light load conditions, as shown in Fig. 16(e). In this case, the benefits derived from the PF mode will be significantly diminished, even the characteristics of the voltage gain, switching frequency range, etc, shown in Fig. 13 are still better than the traditional PO mode.

For the heavy load condition, the voltage gain of the LLC converter is decreased along with the load increasing, as shown in Fig. 2. Hence, it is urgent to improve the capability of voltage gain step-up for the LLC converter under heavy load condition. Therefore, from Fig. 14, when the voltage ringing is higher than zero by detecting the voltages across

SR switches, the LLC converter works at conventional PO mode to keep the high efficiency at the light load condition. For the heavy load and high step-up voltage gain case, when the voltage ringing reach to zero by detecting the voltages across SR switches, the converter can work at PF mode by using the proposed scheme to cover the wide voltage-regulation range, instead of using two-stage converters or adding some auxiliary switches to enhance the voltage-regulation capability.



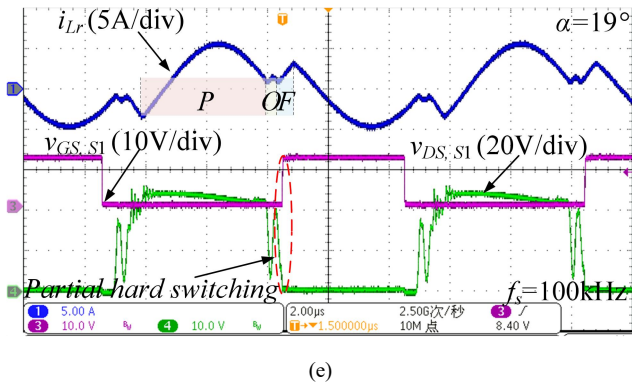


**Fig. 16.** Experimental waveforms at 100kHz switching frequency at (a) & (b)  $V_o=12V/8A$ ,  $V_{in}=75V$ , (c) & (d)  $V_o=12V/8A$ ,  $V_{in}=85V$ , (e)  $V_o=12V/6A$

When the LLC converter operates at the same input voltage, output voltage, and load current, the key waveforms are shown in Fig. 17. When the converter operates at PO mode with  $\alpha=0^\circ$  in Fig. 17(a), and POF mode with  $\alpha=19^\circ$  in Fig. 17(b), the switching frequency is increased from 56kHz to 100kHz. As a sequence, the switching frequency range can be squeezed significantly along with the increased leading angle  $\alpha$ , which is consistent with the theoretical analysis. In addition, according to Fig. 13(a), although 73V minimum input voltage can be achieved theoretically, the partial hard switching occurred in the primary switches due to a very low current at the end of the O stage and caused the voltage spike across the primary switches, as shown in Fig. 17(a). Therefore, the actual minimum input voltage should be at least higher than 85V so that the switching frequency is close to the resonant frequency to increase the current at the end of the O stage, and achieves ZVS turn-on of the primary switches. For this reason, the voltage regulation range of the traditional LLC converter with PO mode is further squeezed and the maximum voltage gain is around

$$G = \frac{2nV_o}{V_{in}} = \frac{2 \times 5 \times 12}{87} = 1.38. \quad (18)$$

As shown in Fig. 17, the peak current  $i_{Lr}$  is 6.5A in the traditional LLC converter with PO mode from Fig. 17(a), while the peak current  $i_{Lr}$  is 5.5A in the proposed LLC converter with POF mode from Fig. 17(b), which verifies that the peak current  $i_{Lr}$  can be reduced by the proposed F stage.

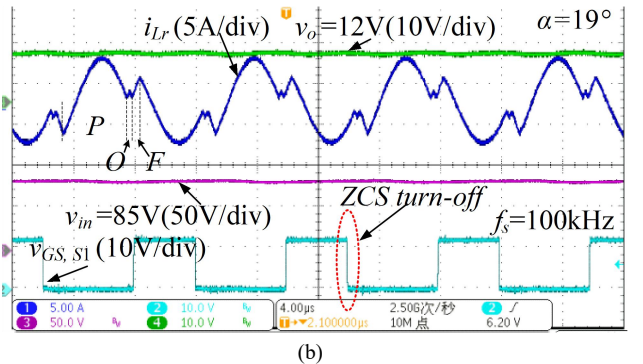
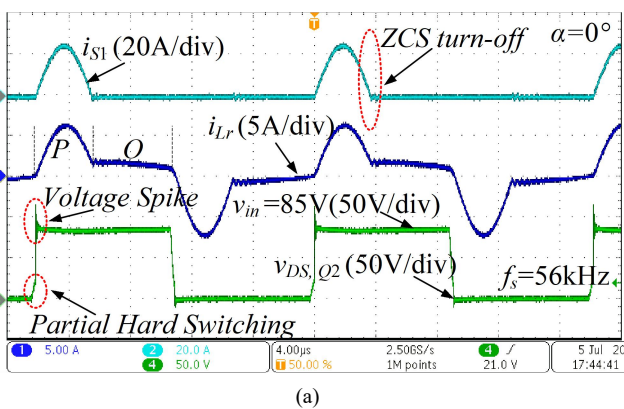
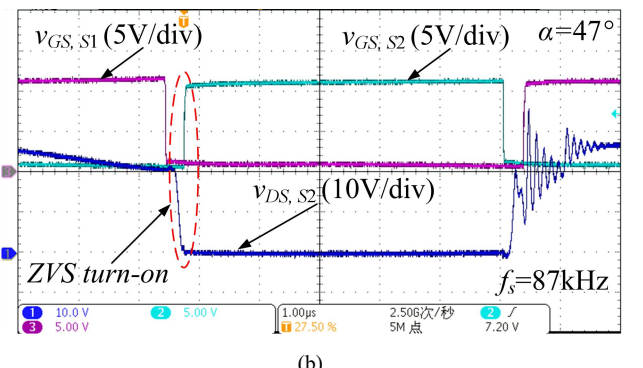
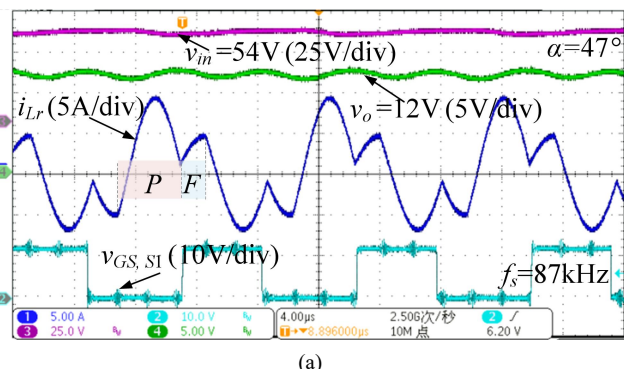


**Fig. 17.** Experimental waveforms at 12V/8A output, and 85V input (a) 56kHz switching frequency under PO mode and  $\alpha=0^\circ$  (b) 100kHz switching frequency under POF mode and  $\alpha=19^\circ$

From Fig. 16(a), the primary switches are turned-on when the F stage ends. According to Fig. 17, when the primary switches are turned on, the primary current  $i_{Lr}$  is increased from 0.3A under conventional PO mode to 3.2A under proposed PF mode at 85V input and 12V/8A output conditions. Therefore, ZVS condition of the primary switches shown in (19) can be satisfied more easier, and thereby reduced dead time of primary switches to improve the efficiency [12].

$$i_{Lr,Q_p,on} t_{dead} \geq 2C_{oss,Q_p} V_{in} \quad (19)$$

where  $i_{Lr,Q_p,on}$  is the resonant current when the primary switches are turned on,  $t_{dead}$  is the dead time of primary switches, and  $C_{oss,Q_p}$  is the output parasitic capacitance of the primary switches.



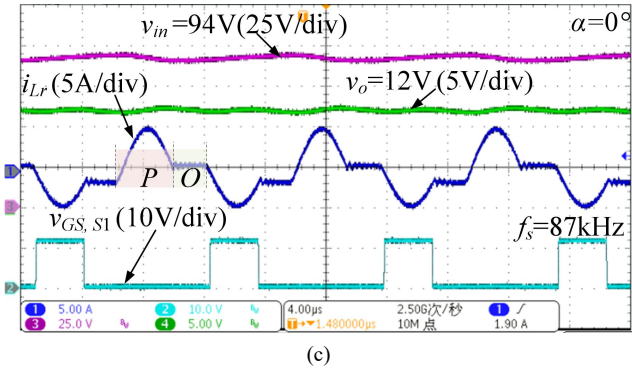


**Fig. 18.** Experimental waveforms at 12V/8A output, and 87kHz switching frequency (a) and (b) at 54V input voltage under PF mode and  $\alpha=47^\circ$ , (c) at 94V input voltage under PO mode and  $\alpha=0^\circ$

Fig. 18 (a) shows that the maximum voltage gain when the converter operates at PF mode with  $\alpha=47^\circ$  in Fig. 18(a), and the maximum voltage gain

$$G = \frac{2nV_o}{V_{in}} = \frac{2 \times 5 \times 12}{54} = 2.22 \quad (20)$$

with 54V input can be achieved at 87kHz switching frequency and 12V/8A output, which is corresponding with the Fig.12 (a). Fig. 18 (b) shows ZVS turn-on of SR switches  $S_1$  and  $S_2$  PF mode with  $47^\circ$  leading angle, which verifies the soft switching characteristic of the proposed scheme. As shown in Fig. 18(c), at the same output and switching frequency condition, the voltage gain is

$$G = \frac{2nV_o}{V_{in}} = \frac{2 \times 5 \times 12}{94} = 1.28 \quad (21)$$

with PO mode. Therefore, at the same load condition, the maximum voltage gain can be improved 1.61 times according to (18) and (20), and the voltage gain can be improved 1.73 times by the proposed novel operation modes at 87kHz switching frequency according to (20) and (21).

TABLE II  
LOSS ANALYSIS OF THE PROPOSED DC-DC CONVERTER

	$I_{Q1,rms}^2 R_{ds(on)} + I_{Q2,rms}^2 R_{ds(on)}$ ( $I_{Q1,rms}$ and $I_{Q2,rms}$ are RMS value of drain-to-source current through switches $Q_1$ and $Q_2$ , $R_{ds(on)}$ is on-state resistance of primary switches)
$P_{Q1} + P_{Q2}$	$\frac{1}{2} t_f V_{in} f_s i_{Lr}(t_6) + \frac{1}{2} t_f V_{in} f_s i_{Lr}(t_2)$ ( $t_f$ is falling time of primary switches)
	$v_g(Q_{g1} + Q_{g2})f_s$ ( $v_g$ is drive voltage of primary switches, $Q_{g1}$ and $Q_{g2}$ are gate charge of switch $Q_1$ and $Q_2$ )
$P_{S1} + P_{S2}$	$I_{S1,rms}^2 R_{ds(on)} + I_{S2,rms}^2 R_{ds(on)}$ ( $I_{S1,rms}$ and $I_{S2,rms}$ are RMS value of drain-to-source current through switches $S_1-S_2$ , $R_{ds(on)}$ is on-state resistance of secondary switches)
	$\frac{V_F}{T_s} (\int_{t_0-t_d}^{t_0} i_{S1} dt + \int_{t_4-t_d}^{t_4} i_{S2} dt)$ ( $t_d$ is conduction time of the body diodes of secondary switches)

$P_{driver}$	$v_g(Q_{g1} + Q_{g2})f_s$ ( $v_g$ is drive voltage of secondary switches, $Q_{g1}$ and $Q_{g2}$ are gate charge of switch $S_1$ and $S_2$ )
$P_{Lr}$	$I_{Lr}^2 R_{ac,Lr}$ ( $R_{ac,Lr}$ and $I_{Lr}$ are the AC resistance, and the AC RMS current of the inductor $L_r$ , respectively)
$P_{core}$	$P_v V$ ( $P_v$ is constants, which are related to material and $\Delta B$ , $V$ is the volume of the core of inductor $L_r$ )
$P_{Tx}$	$I_{Lp}^2 R_{ac,Lp} + I_{Ls}^2 R_{ac,Ls}$ ( $R_{ac,Lp}$ and $I_{Lp}$ are the AC resistance, and the RMS current in primary side; $R_{ac,Ls}$ and $I_{Ls}$ are the AC resistance, and the AC RMS current in secondary side)
$P_{core}$	$P_v V$ ( $P_v$ is constants, which are related to material and $\Delta B$ , $V$ is the volume of the core of transformer $T_x$ )
$P_C$	$I_{C_{in},rms}^2 R_{ESR,Cin} + I_{Cr,rms}^2 R_{ESR,Cr} + I_{Co,rms}^2 R_{ESR,Co}$ ( $R_{ESR,Cin}$ , $R_{ESR,Cr}$ and $R_{ESR,Co}$ are equivalent series resistance of capacitors $C_{in}$ , $C_r$ and $C_o$ . $I_{C_{in},rms}$ , $I_{Cr,rms}$ and $I_{Co,rms}$ are RMS value of the current through capacitors $C_{in}$ , $C_r$ and $C_o$ .)
Auxiliary power supply	Power for controller and ICs, and others (copper loss of the track, etc.)

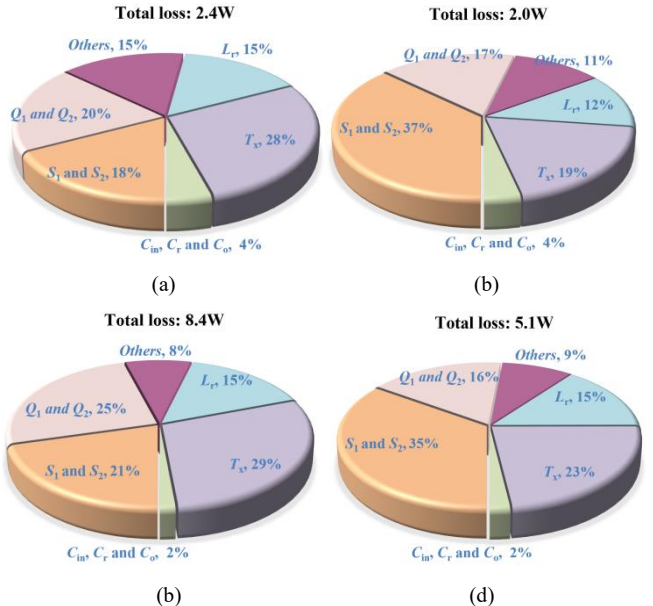


**Fig. 19.** Loss breakdown of the proposed converter at (a)  $V_{in}=115V$ ,  $V_o=12V$ , full load, (b)  $V_{in}=115V$ ,  $V_o=12V$ , half-load, (c)  $V_{in}=60V$ ,  $V_o=12V$ , full load, (d)  $V_{in}=60V$ ,  $V_o=12V$ , half-load.

Table II shows the loss analysis of the proposed converter. Fig. 19 shows the loss breakdown at different voltage-regulation ranges and load conditions. From Fig. 19, the loss proportion of the switches  $S_1$  and  $S_2$  at half-load is much higher than that at full-load as ZVS turn-on may not be achieved at light load, which is consistent with the theoretical analysis in [34] and experimental verification in Fig. 16. Therefore, in scenarios with heavy loads and high step-up voltage gain, the voltage-regulation range can be

extended by the proposed control strategy with high efficiency.

Fig. 20 shows the measured efficiency of the PF mode LLC converter and the PO mode LLC converter under soft switching condition with the same power circuit parameters. Although the efficiency with PF mode is slightly lower than that with PO mode at 12V/8A output, the voltage-regulation range is much wider with PF mode, thereby the minimum input voltage can be extended from around 87V to 54V with ZVS turn-on of all the switches.

Table III gives the comparison of the wide voltage-regulation range LLC dc-dc converters. From Table III, by using a large parallel resonant inductance to reduce the circulating current and achieve soft switching easier in the proposed LLC converter, the voltage-regulation range is extended, and the switching frequency range is squeezed without any auxiliary devices. In addition, the proposed wide-voltage-gain scheme can be adopted in any simple LLC resonant converter topology, and the consistent primary-side or secondary-side switching frequency keeps the temperature among these switches balanced. In summary,

the proposed novel operation mode of the LLC converter provides a simple, low-cost, and effective scheme to improve the voltage-regulation capability of the resonant converter.

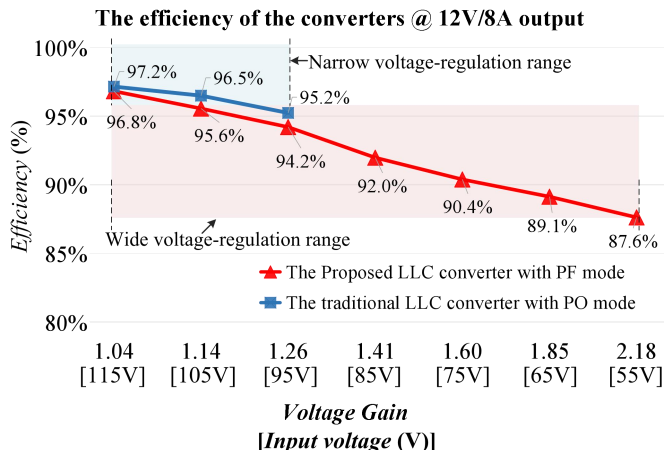


Fig. 20. Measured efficiency

TABLE III: COMPARISON OF THE WIDE VOLTAGE-REGULATION RANGE LLC DC-DC CONVERTERS

References	[10]	[22]	[41]	[42]	This work
Wide voltage-regulation range method	Reduced $k$	Full bridge / half bridge morphing	Reduced $L_m$	Parameter optimization	SR switches turn-on early
Input voltage	320-370	220-760	220-320	370-410	54-115
Output voltage	35-165	400	28	36-72	12
Transformer ratio	22:9	1.125:1	5	4:1:1	20:4:4
Maximum voltage gain	2.52	2.05	1.24	1.57	2.22
Frequency variation range	110 kHz~320 kHz	83kHz~120kHz	792 kHz~1.12MHz	150 kHz~450 kHz	87 kHz~100 kHz
Efficiency	94%	97.8%	96%	96%	96.82%



Fig. 21. Experimental prototype

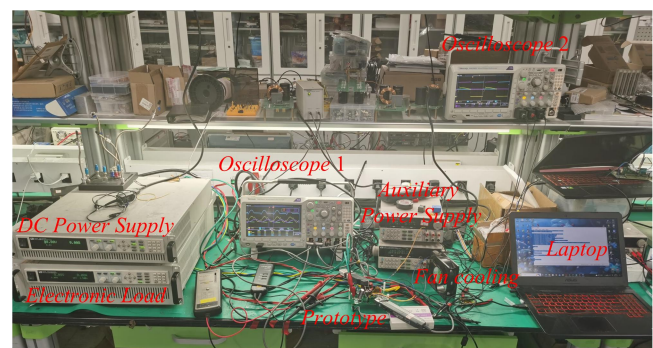


Fig. 22. Testing platform

Fig. 21 shows the experimental prototype of the proposed converter, and Fig. 22 shows the testing platform.

## V. CONCLUSION

Different from the conventional SR LLC converter operation modes consisting of P, O, and N stages, stage F is built and the novel operation modes contained F stage are analyzed in this paper. In the SR LLC converter with the POF or PF mode, the soft-switching of primary and secondary side switches can be achieved, and the advantages of the conventional LLC converter such as simple circuit structure and control strategy are kept. Along with the leading angle  $\alpha$  increasing in the proposed operation modes, the switching frequency range is squeezed and the step-up voltage gain is improved significantly without any added components. In addition, the proposed operation modes can easily extend half-bridge LLC converter, full-bridge LLC converter, or three-level LLC converter, etc, all kinds of SR LLC converters. Therefore, by using the proposed approach, the wide voltage-regulation range with a narrow switching frequency range can be achieved in LLC converter, which overcomes the drawback of LLC converter unsuitable for wide voltage-regulation applications.

## REFERENCES

- [1] J.-W. Kim, B. Kim, D. Lee, Y. Cho, S. K. Ji and D. Ryu, "LLC Resonant Converter for Fast Electric Vehicle Charging Module with a Reconfigurable Bi-Directional Switch," *IEEE Trans. Transport. Electrific.*, 2024. (Early Access)
- [2] B. O. Aarninkhof, D. Lyu, T. B. Soeiro and P. Bauer, "A Reconfigurable Two-Stage 11 kW DC–DC Resonant Converter for EV Charging With a 150–1000 V Output Voltage Range," *IEEE Trans. Transport. Electrific.*, vol. 10, no. 1, pp. 509-522, March 2024.
- [3] C. Sun, R. Wang, X. Xiao, Y. Wang and Q. Sun, "Model-Free Bidirectional Synchronous Rectification Control Scheme for LLC-Based Energy Storage System in Electric-Vehicle Energy Router," *IEEE Trans. Transport. Electrific.*, vol. 9, no. 4, pp. 5140-5150, Dec. 2023.
- [4] G. Xu, S. Luo, J. Xu, W. Xiong, Y. Sun and M. Su, "An ISOP LLC Converter With Changeable Equivalent Magnetizing Inductance Utilizing Coupled Inductor for Ultrawide Input Voltage Range Application," *IEEE Trans. Transport. Electrific.*, vol. 10, no. 2, pp. 3680-3689, June 2024.
- [5] M. I. Shahzad, S. Iqbal and S. Taib, "Interleaved LLC Converter With Cascaded Voltage-Doubler Rectifiers for Deeply Depleted PEV Battery Charging," *IEEE Trans. Transport. Electrific.*, vol. 4, no. 1, pp. 89-98, March 2018.
- [6] E. G. Schmidtner, "A new high-frequency resonant converter topology," in *High Frequency Power Conversion (HFPC) Conference Record*, pp. 390–403, 1988.
- [7] J. F. Lazar and R. Martinelli, "Steady-state analysis of the LLC resonant converter," in *IEEE Appl. Power Electron. Conf. Expo., Anaheim, CA, USA*, pp. 728–735, Mar. 2001.
- [8] B. Yang, F. C. Lee, A. J. Zhang and G. Huang, "LLC resonant converter for front end DC/DC conversion," in *IEEE Appl. Power Electron. Conf. Expo., Dallas, TX, USA*, pp. 1108–1112, Mar. 2002.
- [9] B. Yang, "Topology investigation for front end DC/DC power conversion for distributed power system," *PhD Dissertation*, Virginia Polytechnic Institute and State University, 2003.
- [10] R. Beiranvand, B. Rashidian, M. R. Zolghadri and S. Mohammad H. Alavi, "A design procedure for optimizing the LLC resonant converter as a wide output range voltage source," *IEEE Trans. Power Electron.*, vol. 27, no. 8, pp. 3749-3763, Aug. 2012.
- [11] X. Fang, H. Hu, F. Chen, etc., "Efficiency-oriented optimal design of the LLC resonant converter based on peak gain placement," *IEEE Trans. Power Electron.*, vol. 28, no. 5, pp. 2285–2296, May 2013.
- [12] Y. Wei, Q. Luo, Z. Wang, and A. Mantooth, "A complete step by step optimal design for LLC resonant converter", *IEEE Trans. Power Electron.*, vol. 36 no. 4, pp. 3674 – 3691, Apr. 2021.
- [13] X. Fang, H. Hu, Z. J. Shen and I. Batarseh, "Operation mode analysis and peak gain approximation of the LLC resonant converter," *IEEE Trans. Power Electron.*, vol. 27, no. 4, pp. 1985-1995, Apr. 2012.
- [14] X. Zhou, B. Sheng, W. Liu, Y. Chen, L. Wang, Y.-F. Liu and P. C. Sen, "A high-efficiency high-power-density on-board low-voltage dc-dc converter for electric vehicles (EVs) application", *IEEE Trans. Power Electron.*, vol. 36, no. 11, pp. 12781 – 12794, Nov. 2021.
- [15] R. Beiranvand, B. Rashidian, M. R. Zolghadri, and S. M. H. Alavi, "Using LLC resonant converter for designing wide-range voltage source," *IEEE Trans. Ind. Electron.*, vol. 58, no. 5, pp. 1746-1756, 2011.
- [16] Z. Fang, T. Cai, S. Duan, and C. Chen, "Optimal design methodology for LLC resonant converter in battery charging applications based on time-weighted average efficiency," *IEEE Trans. Power Electron.*, vol. 30, no. 10, pp. 5469-5483, Oct. 2015.
- [17] A. Mustafa and S. Mekhilef, "Dual phase LLC resonant converter with variable frequency zero circulating current phase-shift modulation for wide input voltage range applications," *IEEE Trans. Power Electron.*, vol. 36, no. 3, pp. 2793-2807, Mar. 2021.
- [18] T. Qian and C. Qian, "A combined topology with coupled LLC resonance for wide-range operation," *IEEE Trans. Power Electron.*, vol. 34, no. 7, pp. 6593-6600, Jul. 2019.
- [19] B. Xue, H. Wang, J. Liang, Q. Cao, and Z. Li, "Phase-shift modulated interleaved LLC converter with ultrawide output voltage range," *IEEE Trans. Power Electron.*, vol. 36, no. 1, pp. 493-503, Jan. 2021.
- [20] H. Wang, Y. Chen, P. Fang, etc., "An LLC converter family with auxiliary switch for hold-up mode operation," *IEEE Trans. Power Electron.*, vol. 32, no. 6, pp. 4291-4306, Jun. 2017.
- [21] C. In-Ho, K. Young-Do, and M. Gun-Woo, "A half-bridge LLC resonant converter adopting Boost PWM control scheme for hold-up state operation," *IEEE Trans. Power Electron.*, vol. 29, no. 2, pp. 841-850, Feb. 2014.
- [22] D. Sha, and X. Yang, "Wide voltage input full bridge (FB) / half bridge (HB) morphing based LLC de-dc converter using numerical optimal trajectory control," *IEEE Trans. Ind. Electron.*, vol. 70, no. 4, pp. 3697 - 3707, Apr. 2023.
- [23] Y. Wei, Q. Luo, and H. A. Mantooth, "An LLC converter with multiple operation modes for wide voltage gain range application," *IEEE Trans. Ind. Electron.*, vol. 68, no. 11, pp. 11111-11124, Nov. 2021.
- [24] C. Li, M. Zhou, and H. Wang, "An H5-bridge-based asymmetric LLC resonant converter with an ultrawide output voltage range," *IEEE Trans. Ind. Electron.*, vol. 67, no. 11, pp. 9503-9514, Nov. 2020.
- [25] X. Tang, Y. Xing, H. Wu, and J. Zhao, "An improved LLC resonant converter with reconfigurable hybrid voltage multiplier and PWM-Plus-PFM hybrid control for wide output range applications," *IEEE Trans. Power Electron.*, vol. 35, no. 1, pp. 185-197, Jan. 2020.
- [26] H. Wu, Y. Li, and Y. Xing, "LLC resonant converter with semiactive variable-structure rectifier (SA-VSR) for wide output voltage range application," *IEEE Trans. Power Electron.*, vol. 31, no. 5, pp. 3389-3394, May. 2016.
- [27] P. Rehlaender, O. Wallscheid, F. Schafmeister, and J. Bocker, "LLC resonant converter modulations for reduced junction temperatures in half-bridge mode and transformer flux in the on-the-fly morphing thereto," *IEEE Trans. Power Electron.*, vol. 37, no. 11, pp. 13413 - 13427, Nov. 2022.
- [28] H. Hu, X. Fang, F. Chen, Z. J. Shen, and I. Batarseh, "A modified high-efficiency LLC converter with two transformers for wide input-voltage range applications," *IEEE Trans. Power Electron.*, vol. 28, no. 4, pp. 1946-1960, Apr. 2013.
- [29] D. Shu and H. Wang, "An ultrawide output range LLC resonant converter based on adjustable turns ratio transformer and reconfigurable bridge," *IEEE Trans. Ind. Electron.*, vol. 68, no. 8, pp. 7115-7124, Aug. 2021.
- [30] J.-W. Kim and G.-W. Moon, "A new LLC series resonant converter with a narrow switching frequency variation and reduced conduction losses," *IEEE Trans. Power Electron.*, vol. 29, no. 8, pp. 4278-4287, Aug. 2014.

- [31] K. Kim, H. Youn, J. Baek, Y. Jeong and G. Moon, "Analysis on synchronous rectifier control to improve regulation capability of high-frequency LLC resonant converter," *IEEE Trans. Power Electron.*, vol. 33, no. 8, pp. 7252-7259, Aug. 2018.
- [32] Z. Fang, J. Wang, R. Liu, L. Xiao, J. Zhang, G. Hu, and Q. Liu, "Energy feedback control of light-load voltage regulation for LLC resonant converter," *IEEE Trans. Power Electron.*, vol. 34, no. 5, pp. 4807-4819, May. 2019.
- [33] S. Bagawade, M. Pahlevani, and P. Jain, "Novel resonant power feedback dc-dc converter," *IEEE Trans. Power Electron.*, vol. 38, no. 3, pp. 4072-4091, Mar. 2023.
- [34] X. Zhou, L. Wang, Y. Gan, H. Luo, Y. -F. Liu, and P. C. Sen, "Accurate analysis and design of the circuit parameters of LLC dc-dc converter with synchronous rectification," *IEEE Trans. Power Electron.*, vol. 37, no. 12, pp. 7252-7259, Dec. 2022.
- [35] MnZn Ferrite Material (EPCOS N87) Datasheet. U.S. Department of Energy - National Energy Technology Laboratory, Sep. 2018.
- [36] Y. Li, Q. Wu, L. Liu, Z. Zhu, "An adaptive constant voltage control scheme for primary-side controlled Flyback converter," *IEEE Trans. Ind. Electron.*, vol. 70, no. 7, pp. 6776 - 6785, Jul. 2023.
- [37] J. Zhang, H. Zeng and X. Wu, "An adaptive blanking time control scheme for an audible noise-free quasi-resonant Flyback converter," *IEEE Trans. Power Electron.*, vol. 26, no. 10, pp. 2735-2742, Oct. 2011.
- [38] C. Wang, S. Xu, W. Shen, S. Lu and W. Sun, "A single-switched high-switching-frequency quasi-resonant Flyback converter," *IEEE Trans. Power Electron.*, vol. 34, no. 9, pp. 8775-8786, Sep. 2019.
- [39] J. Park, Y. Moon, M. Jeong, J. Kang, S. Kim, J. Gong, C. Yoo, "Quasi-resonant (QR) controller with adaptive switching frequency reduction scheme for Flyback converter," *IEEE Trans. Ind. Electron.*, vol. 63, no. 6, pp. 3571-3581, Jun. 2016.
- [40] H. Park, J. Jung, "Modeling and feedback control of LLC resonant converters at high switching frequency," *J. Power Electron.*, vol. 16, no. 3, pp. 849-860, May. 2016.
- [41] De Juan, D. Serrano, P. Alou, J. -N. Mamouss, R. Deniéport and M. Vasic, "High-frequency LLC converter with narrow frequency variations for aircraft applications," *2022 IEEE Applied Power Electronics Conference and Exposition (APEC)*, 2022, pp. 2098-2105.
- [42] F. Musavi, M. Craciun, D. S. Gautam, W. Eberle, and W. G. Dunford, "An LLC resonant dc-dc converter for wide output voltage range battery charging applications," *IEEE Trans. Power Electron.*, vol. 28, no. 12, pp. 5437-5445, 2013.



**Xiang Zhou** (S'16-M'18-SM'23) received the B.S. and Ph.D. degrees in electrical engineering from Southwest Jiaotong University, Chengdu, China, in 2013 and 2018, respectively.

From June 2018 to December 2019, he was with the Department of Electrical and Computer Engineering, Queen's University, Kingston, ON, Canada, as a Post-Doctoral Research Fellow. Since 2019, he has been with Xi'an Jiaotong University, where he is currently an Associate Research Fellow with the School of Electrical

Engineering.

His research interests include soft switching dc-dc and dc-ac converter topology and control strategy, and high-efficiency high-power-density converter design with wide bandgap devices.



**Jiarui Wu** (Student Member, IEEE) was born in Sichuan, China, in 1996. He received the B.S. degree in electrical engineering and automation from the Northeast Forestry University, Harbin, China, in 2019. He received the Ph.D. degrees in electrical engineering from Xi'an Jiaotong University, Xi'an, China, in 2024.

His main research interests include high-frequency magnetics and high power density converter.



**Huan Luo** (M'20) received the B. S. degree in electrical engineering from Southwest Jiaotong University, in 2012, and the M. S. degree in electrical engineering from Sichuan University in 2015, and the Ph. D degree in electrical engineering from Southwest Jiaotong University, in 2020, respectively. He is currently an Associate Professor with the College of Electrical Engineering, Sichuan University. His research interests include the control technique of switching-mode power supplies, single-phase power factor correction and resonant converters.



**Zihao Song** was born in Shandong, China, in 2001. He received the B.S. degree in electrical engineering from Harbin Institute of Technology, Weihai, China, in 2024. He is currently working toward the M.S. degree at Xi'an Jiaotong University.

His research interests include soft switching dc-dc converter and dc-ac converter topology and control.



**Long Pei** (Student Member, IEEE) was born in Hunan, China, in 1995. He received the B.S. degree in electrical automatization in 2018 from Xi'an Jiaotong University, Xi'an, China, where he is currently working toward the Ph.D. degree in electrical engineering and automation.

His research interests include on-board charge, design and control of dc-dc resonant power converters, and power factor correction ac-dc converters.



**Donghua Duan** (Student Member, IEEE) was born in Jiangxi, China, in 2000. He received the B.S. degree in electrical automatization in 2022 from Xi'an Jiaotong University, Xi'an, China, where he is currently working toward the M.S. degree in electrical engineering and automation.

His research interests include design and control of dc-dc resonant power converters, machine learning and intelligent systems and applications, big data applications.



**Peng Guo** (M'22) was born in Hunan, China, in 1992. He received the B.S. degree in electrical engineering from the Wuhan University of Technology, Wuhan, China, in 2015, and the Ph.D. degree in electrical engineering from Hunan University, Changsha, China, in 2020.

He was a Postdoctoral Fellow with Hunan University from 2020 to 2023, where he is currently an Associate Professor with the College of Electrical and Information Engineering. His research interests include switch-mode power amplifier, data-driven nonlinear control, electromagnetic sensing and electromagnetic compatibility for high-frequency power electronics systems.



**Laili Wang** (S'07-M'13-SM'15) received the B.S., M.S., and Ph.D. degrees from the School of Electrical Engineering, Xi'an Jiaotong University, Xi'an, China, in 2004, 2007, and 2011, respectively. Since 2011, he has been a Postdoctoral Research Fellow with the Department of Electrical Engineering, Queen's University, Kingston, ON, Canada. From 2014 to 2017, he was an Electrical Engineer with Sumida, Kingston, ON, Canada. In 2017, he became a Full Professor of Xi'an Jiaotong University. His research interests include Wide Bandgap Power Semiconductors, Packaging & Integration, High Density Power Conversion. He has published more than 240 papers in IEEE journals and conferences, and has been issued 45 Chinese patents and 5 US patents.

## IEEE Transactions on Transportation Electrification

Laili Wang has been rewarded the Gold Medal Award of Geneva Inventions, the First Prize Award of Science and Technology Progress of China Power Supply Society (CPSS), the First Prize of Technical Invention of China Electrotechnical Society (CES), the Second Prize Award of Natural Science of Shaanxi Province. He is also the recipient of National Science Fund for Distinguished Young Scholars, Shaanxi Youth Science and Technology Award, Outstanding Youth Award of China Power Supply Society (CPSS), Youth Science and Technology Award of China Electrotechnical Society (CES), China Electric Power Excellent Young Technological Talent Award of Chinese Society of Electrical Engineering (CSEE).

Laili Wang is currently an Associate Editor for IEEE TRANSACTIONS ON POWER ELECTRONICS and IEEE JOURNAL OF EMERGING AND SELECTED TOPICS IN POWER ELECTRONICS. He is the Co-Chair of System Integration and Application in International Technology Roadmap for Wide Band-Gap Power Semiconductor (ITRW), the Chair of IEEE PELS and CPSS Joint Chapter in Xi'an, Vice Chair of IEEE PELS Membership Committee-China. He is also Vice Chair of the four committees in China Power Supply Society (CPSS).



**Yan-Fei Liu** (M'94–SM'97–F'13) received his Bachelor and Master degree from the Department of Electrical Engineering from Zhejiang University, China, in 1984 and 1987 and PhD degree from the Department of Electrical and Computer Engineering, Queen's University, Kingston, ON, Canada, in 1994.

He was a Technical Advisor with the Advanced Power System Division, Nortel Networks, in Ottawa, Canada from 1994 to 1999.

Since 1999, he has been with Queen's University, where he is currently a Professor with the Department of Electrical and Computer Engineering. His current research interests include optimal application of GaN and SiC devices to achieve small size and high efficiency power conversion, 99% efficiency power conversion with extremely high power density, digital control technologies for high efficiency, fast dynamic response dc–dc switching converter and ac–dc converter with power factor correction, resonant converters and server power supplies, and LED drivers. He has authored around 250 technical papers in the IEEE Transactions and conferences, and holds 35 U.S. patents. He has written a book on "High Frequency MOSFET Gate Drivers: Technologies and Applications", published by IET. He is also a Principal Contributor for two IEEE standards. He received "Modeling and Control Achievement Award" from IEEE Power Electronics Society in 2017. He received Premier's Research Excellence Award in 2000 in Ontario, Canada. He also received the Award of Excellence in Technology in Nortel in 1997.

Dr. Liu was the Vice President of Technical Operations of IEEE Power Electronics Society (PELS, from 2017 to 2020). Dr. Liu serves as an Editor of IEEE JOURNAL OF EMERGING AND SELECTED TOPICS OF POWER ELECTRONICS (IEEE JESTPE) since 2013. He was the General Chair of ECCE 2019 held in Baltimore, USA in 2019. His major service to IEEE is listed below: a Guest Editor-in-Chief for the special issue of Power Supply on Chip of IEEE TRANSACTIONS ON POWER ELECTRONICS from 2011 to 2013; a Guest Editor for special issues of JESTPE: Miniaturization of Power Electronics Systems in 2014 and Green Power Supplies in 2016; as Co-General Chair of ECCE 2015 held in Montreal, Canada, in September 2015; the Chair of PELS Technical Committee (TC1) on Control and Modeling Core Technologies from 2013 to 2016; Chair of PELS Technical Committee (TC2) on Power Conversion Systems and Components from 2009 to 2012.